HAL
open science

Tailoring the rheology and electrical properties of polyamide 66 nanocomposites with hybrid filler approach: graphene and carbon nanotubes

Jordana Palacios, Achraf Ben Fekih, Cristina Yus Argon, Silvia Irusta, Simon Jestin, Sylvie Dagréou

To cite this version:

Jordana Palacios, Achraf Ben Fekih, Cristina Yus Argon, Silvia Irusta, Simon Jestin, et al.. Tailoring the rheology and electrical properties of polyamide 66 nanocomposites with hybrid filler approach: graphene and carbon nanotubes. Polymer international, 2021, 70, pp.1329-1343. 10.1002/pi.6204 . hal-03176040

HAL Id: hal-03176040

https://univ-pau.hal.science/hal-03176040v1

Submitted on 10 Oct 2022

HAL is a multi-disciplinary open access archive for the deposit and dissemination of scientific research documents, whether they are published or not. The documents may come from teaching and research institutions in France or abroad, or from public or private research centers.

L'archive ouverte pluridisciplinaire **HAL**, est destinée au dépôt et à la diffusion de documents scientifiques de niveau recherche, publiés ou non, émanant des établissements d'enseignement et de recherche français ou étrangers, des laboratoires publics ou privés.

TAILORING THE RHEOLOGY AND ELECTRICAL PROPERTIES OF PA66 / NANOCOMPOSITES WITH HYBRID FILLER APPROACH: GRAPHENE AND CARBON NANOTUBES

Jordana K. Palacios[1,2], Achraf Ben Fekih[1], Cristina Yus[3,4], Silvia Irusta[3,4], Simon Jestin[5], Sylvie Dagréou[1]

[1] CNRS/ UNIV Pau & Pays Adour/ E2S-UPPA, Institut Des Sciences Analytiques et de Physico-Chimie Pour l'Environnement et les Materiaux (IPREM), UMR5254, 64000, Pau, France.

[2] Fundación Centro Tecnológico Miranda de Ebro (CTME), R&D Materials Department, Miranda de Ebro, 09200, Burgos, Spain.

[3] Instituto de Nanociencia y Materiales de Aragón (INMA), CSIC-Universidad de Zaragoza, Zaragoza 50009, Spain.

[4] Department of Chemical and Environmental Engineering, University of Zaragoza,50018 Zaragoza, Spain.

[5] CANOE / Le Centre Technologique Nouvelle-Aquitaine Composites et Matériaux Avancés- 16 avenue Pey Berland, 33600 PESSAC, France.

Correspondence to: Jordana K. Palacios (E-mail: *jordanapalacios@ctme.es*)

((Additional Supporting Information may be found in the online version of this article.))

ABSTRACT

The aim was to improve the processability and reduce the melt viscosity of well-known nanocomposites based on polyamide 66 (PA66) and carbon nanotubes (CNT), while keeping the good electrical conductive ability gained after the addition of CNT. Thus, a nanocomposite based on PA66 as the thermoplastic matrix and 3% of CNT was selected. At this composition, a percolated network is created and the material is electrically conductive. The approach followed was the addition of graphene nanoplatelets (GNP) of two different lateral sizes to obtain a PA66 nanocomposite with hybrid filler: CNT/GNP. In addition, third nanocomposite of PA66 with GNP only was prepared for comparison purposes. The rheological characterization determined that adding 1% of GNP of 2 μm particle size decreased the viscosity of the system in 87%. However, the electrical properties were diminished to some extent, from 10^{-5} to 10^{-9} S/cm approximately. The Cross Rheology Model described successfully the experimental rheological data. The CNT/GNP nanocomposite exhibited faster relaxations, almost in 4 orders of magnitude, in comparison with the CNT nanocomposite but slower than the GNP nanocomposite. The nanoparticles improved the crystallization ability of PA66 acting as nucleating agents and increasing the PA66 crystallization temperature in almost 10°C. Self-nucleation experiments demonstrated a supernucleation feature of the hybrid filler. The nucleation efficiency was about 500 %.

INTRODUCTION

Polymer nanocomposites have been in the focus of researchers from the last few decades due to the improvements in the mechanical, thermal, electrical, permeability and thermo-degradability performance. The nanofillers more commonly employed include organoclay, silica nanoparticles, titanium oxide, carbon nanotubes (CNT), expanded graphite, graphite oxide, graphene nanoribbons, graphene nanoplatelets (GNP), among others. Moreover, a novel approach considers the addition of two types of nanoparticles in order to create a synergistic effect between them[1-8].

The viscoelastic behavior in the linear regime of CNT and GNP nanocomposites implies a transition from liquid-like to solid-like response as the nanofiller content increases. The concentration corresponding to this transition is the so-called rheological percolation threshold. Below the percolation threshold, the nanofillers should be well dispersed and they will act as isolated objects inside the polymer matrix. Thus, the material retains the same viscoelastic behavior as the polymer matrix. As nanofiller content increases, the percolation limit is reached and a network develops and dominates the mechanical response. The percolated network restricts the segmental motions of the polymer chains near the nanoparticle interphase and the storage modulus (G') shows a plateau in the low frequency region. At very high nanofiller concentrations, beyond the percolation threshold, the effect on the rheological response is lower. The ranges of rheological and electrical percolation thresholds, reported in literature, are very wide and depend on the quality of dispersion, the nanofillers size and shape, their concentration and orientation, chemical modifications, mixing conditions, particle-particle interconnections, polymer-polymer entanglements and polymer-particle interactions[9]. The difference between GNP and CNT relies on their size and aspect ratio. Increment on viscosity has been reported after the addition of CNT or GNP to polymer matrices. However, the viscosity increment of GNP composites is not as big as in CNT nanocomposites. Additionally, higher percolation thresholds have been reported for GNP nanocomposites, in comparison to CNT nanocomposites[9,10]. The material does not flow and behaves as a solid due to the formation of an interconnected CNT network.

Additionally, GNP and CNT are suitable to fabricate conductive nanocomposites. The carbon nanofillers can form conductive percolated pathways for electron transfer, employing small nanoparticle content. GNP can provide conductivity at significantly lower loading than

other carbon fillers but its improvement is not as good at the one obtained with CNT nanofillers[9-11]. This is an indication of the better quality of the percolated network formed by the CNT.

Different polymer matrices, mixed with either GNP or CNT, have been evaluated. For instance, GNP increased the Newtonian viscosity of epoxy matrix nanocomposites.[11] On the contrary, the addition of CNT to epoxy matrix induced a loss of the Newtonian plateau and an increase of the viscosity at low frequencies. In the high frequency region, the CNT can align and flow with the polymer matrix, exhibiting a shear thinning behavior, due to the CNT network breakdown caused by the high shear rate. Thus**,** it is clear that the nanoparticle shape influences the rheological behavior of the polymer matrix[11,12]. For instance, Knauert et al.[12] have performed some theoretical simulations to compare the effect of spherical, rod and sheet-like nanoparticles. From their results, the 1D rod-shape nanoparticles (as in CNT) promoted a larger increase in viscosity than the 2D sheet-like nanoparticles (as in GNP), probably due to the higher polymer-particle interactions favored by the CNT nanofiller network. Therefore, a combined strategy has been proposed in order to address the rise of the viscosity and to gain the best features of both nanoparticles. With that purpose, the simultaneous use of both CNT and GNP as a hybrid filler have been evaluated in different type of matrices, from thermosetting to thermoplastics ones[1-5], as well as into polymer blends[13].

For instance, Prolongo et al.[1] evaluated the simultaneous addition of both CNT and GNP to an epoxy matrix. The electrical conductivity of the CNT/GNP nanocomposites was in between the electrical conductivity of the nanocomposites with only GNP and the nanocomposites with CNT, which was the highest. Similarly, the viscosity of the hybrids CNT/GNP nanocomposites was higher than that of the GNP systems but lower than the viscosity in the CNT nanocomposites. The authors presented a hybrid filler nanocomposite with a good compromise between electrical and thermal conductive properties. Similar behavior was observed by Araby et al.[3] in EPDM/GNP/CNT nanocomposites. The authors attributed this synergistic effect to a bridge-linking role of the CNT among the GNP flakes through π–π interactions. Other authors as Rostami et al.[14] have reported similar results as well. The simultaneous addition of CNT and GNP to a TPU matrix contributed to enhance the ultimate electrical, thermal and mechanical properties. Intermediate values of viscosity

and electrical conductivity were reported for the hybrid systems and the rheological percolation was achieved. Similarly, Infurna et al.[15] reported an increased viscosity in polypropylene (PP) nanocomposites with both CNT and GNP in different ratios, in comparison to the viscosity of the binary PP/GNP systems. Additionally, a synergistic effect on the electrical behavior was observed with the addition of the two nanoparticles indicating interconnected paths. However, the authors evaluate the rheological response in the range of high shear rates (i.e beyond 5 up to 100 s^{-1}) and therefore no information about percolation (which is detected at the low frequency region) is reported.

On the other hand, Xiao et al.[4] prepared poly(vinylidene fluoride) (PVDF) nanocomposites mixed with GNP and CNT. Although, the crystallinity values remained almost unchangeable, both carbon nanoparticles promoted excellent nucleation for the crystallization of the PVDF matrix. The PVDF/CNT/GNP nanocomposites had improved conductivity, in comparison to the PVDF/GNP system, but the values are still lower than that of the PVDF/CNT system. Also, the hybrid filler PVDF/CNT/GNP nanocomposites exhibited a solid-like response and an increased viscosity while the PVDF/GNP system exhibited a rheological response similar to that of pure PVDF. Other authors proposed the hybrid filler approach of the carbon nanoparticles but with other types of inorganic nanofillers. For instance, Feng et al.[16] reported improved thermal conductivity and crystallinity of polyethylene (PE) nanocomposites containing both CNT and boron nitride particles. In addition, a clearer solid like response was observed in the rheological behavior of the hybrid filler composites in comparison to the binary system including only the boron nitride fillers, indicating the formation of filler network structure. The authors established a relationship between the thermal conductivity and the rheological features.

Particularly for polyamides (PA), several authors have tried to elucidate the effect of the nanoparticles interactions in the final properties of PA66 (or PA6) hybrids filler nanocomposites with CNT, GNP and other types of carbon nanofillers such as expanded graphite, graphite oxide, carbon black, carbon fibers, among others[17-20]. PAs are of great interest due to their good properties. They have high tensile, flexural, compressive, and shear strength as a cause of their crystallinity [21], but they are also tough above their glass transition[22]. Particularly, PA66 (or PA6) nanocomposites with CNT or GNP exhibited improved mechanical, barrier and electrical properties, better thermal stability and

conductivity, unchanged[23] or increased [24-26] crystallinity and crystallization temperature, a nanofiller nucleating effect[23-29] but also increased viscosity and the expected solid-like response (at low frequencies)[23,26,30]. The electrical and rheological percolation thresholds, reported in literature for these nanocomposites, are very wide. Both of them are much higher in the GNP nanocomposites than in the nanocomposites with CNT[25].

Therefore, the CNT/GNP hybrid approach has also been considered for PA66 (or PA6) nanocomposites. For instance, Doagou-Rad et al.[31] and Kim et al.[17] evaluated the addition of GNP and CNT to a PA66 matrix. Employing different GNP/CNT ratio compositions, both authors claimed that the addition of a quantity of GNP in a PA66/CNT nanocomposite improved its mechanical performance to some extent, in terms of Young modulus, yield stress, hardness, tensile strength, while thermal conductivity could be diminished [31]. As in other hybrid nanocomposites, the effect of the CNT in the rheological behavior was more pronounced than that of the GNP. Also, the solid-like behavior, typically observed in CNT nanocomposites, became less significant with the addition of the GNP. Similarly, lower storage modulus and viscosity values have been observed in PA6 hybrid nanocomposites including both carbon black and CNT, in comparison with binary PA6/CNT nanocomposites of similar total filler content [18].

Doagou-Rad et al. [31] also claimed an increase in the crystallization temperature of PA6 matrix caused by a nucleation action of the nanoparticles. However, the crystallinity degree was not significantly increased. Similar results were observed in PA6 hybrid filler nanocomposites with both CNT and carbon black[18] and both CNT and expanded graphite (EG) [32].

The electrical behavior of nanocomposites including CNT have been widely researched for different polymeric matrixes such as polypropylene, poly(L-lactide), poly(oxymethylene) and properties like electrical conductivity and electromagnetic interference shielding have been studied[7,8]. Particularly, for PA matrixes, Zhu et al.[33] reported an improved electrical conductivity in PA6/CNT nanocomposites reinforced with carbon fibers. However, high total nanoparticle content (up to 11 %) was needed to observe a synergistic effect between the two types of carbon nanofillers. An effective conductive network is strictly related to a uniform distribution of the nanofillers in the polymer matrix. If the nanofillers are very well dispersed and distributed, lower nanofillers content are

required to properly conduct the electrical chargers. Ultimately, the CNT could act as electric bridges between the carbon fibers, allowing the electro transfer through the polymer matrix. H K. Feng Cheng et al. [18] also reported a synergistic effect on the electrical conductivity properties in PA6 hybrid nanocomposite with a CNT/Carbon black composition of 10/10%. Similarly, good electrical conductivity properties were reported by Chen et al.[6] in PCL nanocomposites that include both CNT and graphene oxide. The best electrical behavior was observed in the PCL nanocomposite with CNT:graphene oxide ratio of 4:1, which was also the system that exhibited less particle aggregation.

The hybrid filler approach might offer better final properties to a PA66 matrix. Besides the Doagou-Rad et al.[31] and Kim et al.[17] reports, not other works have been published regarding PA66 hybrid nanocomposites with GNP and CNT. These authors only describe the rheological and crystallization behavior without making emphasis in the phenomena behind them. Here we present a detailed rheological study of PA66 / Hybrid filler nanocomposites, which was also analyzed in terms of the Modified Cross Model. Additional electrical conductivity measurements are presented. Moreover, the quality of the hybrid nanofiller system as nucleating agent for crystallization is addressed in terms of Self-nucleation experiments. The addition of organic or inorganic fillers will modify the flow behavior of the polymer matrix. Therefore, understanding the rheological behavior of the systems is mandatory to address the best procedures and work conditions during melt processing.

EXPERIMENTAL

Materials

Polyamide 66 (PA66) from Solvay (TECHNYL® A 205F, injection grade, ρ = 1.14 g cm^{-3}), was used as polymer matrix. Two types of carbon nanofillers were employed: multi-wall carbon nanotubes (CNT from ARKEMA (Graphistrength® C100)) and graphenes nanoplatelets (GNP from XG-Sciences). The CNT have apparent density of 50-150 kg/m^3 and the following dimensions: 10-15 nm of diameter and 0.1-10 μm of length. Two GNP of different lateral size, surface area and thickness were selected: C750 (2 μm, 750 m^2 g^{-1} and 2 nm, denoted as GNP-2) and M25 (25 μm, 120-150 m^2 g^{-1} and 6-15 nm, denoted as GNP-25). The carbon nanofillers were used as received.

Nanocomposites preparation

The hybrid CNT/GNP nanocomposites were prepared by melt extrusion in a twin screw extruder model LAB TECH ENGINEERING COMPANY LTP. The screw rate was 100 rpm and the temperature profile from the die to the extrusion zone was 255-270-285-280-270-220-150 °C. Prior to extrusion, the PA66 was dried under continuous vacuum during 17 h at 80 °C. The CNT and GNP nanoparticles were first physically mixed and then added to the PA66 pellets. Then, the whole mixture was extruded. A fixed content of CNT (3 wt%) and a variable quantity of GNP (from 0.25 to 1 %) were added. Equivalent binary nanocomposites with only 3 and 4 wt% of GNP or CNT were prepared for comparison purposes. Table 1 summarizes the compositions of the samples. The nanocomposites with only CNT or GNP will be referred as binary nanocomposites, while those nanocomposites that include both CNT and GNP nanofillers will be referred as hybrid filler nanocomposites. The number at the end of the designation indicates the size of the GNP nanoparticles.

Table 1: Composition of the nanocomposites

System	Samples	CNT Content (wt%)	GNP-2 Content (wt%)	GNP-25 Content (wt%)	Total filler content (wt%)
Pure PA	PA66	-	-	-	0.00
Carbon nanotubes nanocomposites	3.00-CNT	3.00	-	-	3.00
	4.00-CNT	4.00	-	-	4.00
Graphene nanocomposites	4.00-GNP-2	-	4.00	-	4.00
	4.00-GNP-25	-	-	4.00	4.00
Hybrid filler nanocomposites:	3/0.25-CNT/GNP-2	3.00	0.25	-	3.25
	3/0.50-CNT/GNP-2	3.00	0.50	-	3.50
	3/0.75-CNT/GNP-2	3.00	0.75	-	3.75
	3/1.00-CNT/GNP-2	3.00	1.00	-	4.00
	3/0.25-CNT/GNP-25	3.00	-	0.25	3.25
	3/0.50-CNT/GNP-25	3.00	-	0.50	3.50
	3/0.75-CNT/GNP-25	3.00	-	0.75	3.75
	3/1.00-CNT/GNP-25	3.00	-	1.00	4.00

Morphology

The morphology of the nanoparticles dispersed in the PA66 matrix was observed by a FEI Inspect F50 field emission gun scanning electron microscope operated at 10kV. Prior to observation, the samples were cryogenic fractured and carbon coated in a Leica EM ACE200 coater.

Rheology

The rheological behavior of the hybrid and binary nanocomposites was evaluated by dynamic rheological measurements in the linear regime. The materials were compression molded into disks of 25 min diameter, and 2 mm thickness. Prior to tests, the specimens were dried under continuous vacuum during 17 h at 80 °C. An ARES TA Instrument Rheometer with a parallel plate geometry was employed. Time sweeps at a constant frequency of 10 rad s^{-1} were performed to analyze the stability of the nanocomposites during the tests. Frequency sweep tests were carried out under nitrogen atmosphere. The test temperature was 275 °C and 5 % of strain was imposed after having previously confirmed that the 5 % value belong to linear regime behavior of the material. The samples were previously heated at 275 °C during 3 min to ensure the complete melting of PA66 matrix, and then the spectromechanical analysis was conducted.

Cross Model

A modified Cross Model[34] including a yield stress[35] was used to fit the experimental viscosity values in the low frequency region. Through equation 1, this model is capable to fit the viscosity increment at low frequencies, which is typically observed in nanocomposites. After fitting, 4 parameters can be determined: the zero shear viscosity, η_0, the yield stress, σ_0, the relaxation time, τ and the pseudoplasticity index, n.

$$\eta(\omega) = \frac{\sigma_0}{\omega} + \frac{\eta_0}{[1 + (\tau\omega)^n]} \qquad Eq.1$$

The parameters were obtained by χ^2 minimization by means of the Nelder-Mead simplex method [36], following the procedure reported by Charman et al [35]. The objective function is defined by equation 2. Seed values of the four parameters are supplied. The convergence criterion for the iterations was when the absolute change in two successive χ-values was lower than 10^{-4}.

$$(\chi)^2 = \frac{1}{n_{exp}}\left(\sum_{i=1}^{n_{exp}} \frac{\left[log\left(n_{exp,i}\right) - log\left(n_{theor,i}\right)\right]^2}{\left[log\left(n_{exp,i}\right)\right]^2}\right) \qquad Eq.2$$

Differential Scanning Calorimetry

Samples of approximately 5 mg were encapsulated in aluminum pans and tested in a TA Instrument Q100 under ultra-high purity nitrogen atmosphere. The instrument was previously checked with an indium standard. All the samples were dried before testing for 17 h at 80 ºC under continuous vacuum. The thermal protocols employed to study the crystallization behavior of the samples are described below.

Standard DSC experiments

All the samples in Table 1 were tested employing standard DSC measurements. The thermal program was as follows: an initial heating run from 50 to 280 °C at 20 °C min^{-1} keeping the sample for 3 min at that temperature to erase the thermal history, followed by a

cooling scan down to 50 °C at 20 °C min^{-1}, and a second heating scan up to 280 °C also at 20 °C min^{-1}.

Self-nucleation experiments

The PA66 were selected to conduct self-nucleation (SN) experiments to evaluate efficiency of the carbon nanofillers as nucleating agents. The self-nucleation thermal protocol was first proposed by Fillon et al.[37,38] and has been extensively used by Müller et al. who have recently published a review about the technique[39]. The aim is to produce self-nuclei by partial melting of a standard crystalline state [40]. The thermal protocol is described as follows: (a) erasure of previous thermal history and crystalline memory by heating the sample up to 280 ºC for 3 min; (b) controlled cooling down to 50 ºC at 20 ºC min^{-1} to create a standard crystalline state (the sample was kept at 50 ºC for 1 min); (c) heating up to a self-nucleation temperature (T_s) at 20 ºC min^{-1}; (d) isothermal step at T_s for 5 min; (e) DSC cooling scan from T_s down to 50 ºC at 20 ºC min^{-1} to record the effect of the thermal treatment at T_s on the PA66 crystallization (the sample was kept at 50 ºC for 1 min); and (f) DSC heating scan from 50 ºC up to 280ºC, to record the PA6 melting after the entire treatment.

From the SN experiments, the *Domains* of Self-Nucleation can be determined. Depending on the T_s chosen, the polymer can melt entirely, only self-nucleate or self-nucleate and anneal. If the T_s is high enough, the polymer melts completely and no crystalline memory is left (the crystallization (T_c) and melting (T_m) temperatures remain unchanged). Those T_s temperatures belong to *Domain I*.

In *Domain II*, the melt is no longer isotropic and two possible situations can be considered. In the high temperature range within *Domain II*, the melt retains some residual chain segmental orientation, or crystalline memory that causes self-nucleation. In the low temperature range within *Domain II,* small fragments of crystals remain that cannot be annealed during the time spent at T_s [39].

When the T_s is low enough, the material melts only partially and a significant amount of crystals remain unmolten. These unmolten crystals can anneal during the 3 min holding time at Ts. A characteristic annealing peak will then appear in the subsequent melting scan, revealing *Domain III.*

Electrical conductivity measurements

Electrical conductivity measurements were performed in electrometer Keithley 6517B. The specimens were squares prepared by compression molding of 3 mm thickness and 3 cm lateral side. Two electrodes were painted with silver paint. The resistance values were averaged out over 3 valid measurements. The electrical conductivity was then calculated from the following equation:

$$\sigma = \frac{l}{RS}$$

where l is the distance between electrodes, R is the resistance in Ω and S is the transversal section area, which in this case is the thickness of the specimen multiplied by the lateral dimension.

RESULTS AND DISCUSSIONS

In general, PA66 (or PA6) nancomposites with CNT exhibit a good balance of properties with respect to the polymer matrix: improved mechanical performance, enhanced crystallinity thermal stability, and enhanced electrical performance. The electrical percolation thresholds have been reported in a wide range, going from less than 1 % to very high contents, up to 7 %. The final value will depend in several factors that include the quality of the dispersion and mixing process and the particle-particle interactions. This percolation threshold can go to even higher values (beyond 10 %) when only GNP are used as nanofillers to provide an electrical feature the polymeric matrix.

The main issue with the use of CNT is the increment in the viscosity obtained after their addition. The aim was to obtain an electrical conductive PA66 nanocomposite with reduced viscosity, using both GNP and CNT. Thus, we decided to first determine the electrical percolation threshold of a PA66/CNT binary nanocomposite. To that purpose, we prepared PA66 nanocomposites with 0.5, 1, 2, 3, 4 and 5 % of CNT. After electrical conductive measurements and rheological evaluations (results no shown, see Figure S1 and S2 in Supplementary Information), we determined that a PA66 nanocomposite with 3 % of CNT exhibited a percolated network: a crossover of *G'* over *G''* at low frequencies and a significant increment in the electrical conductivity value that indicated that a minimum electrical threshold have been reached. Therefore, we have chosen a PA66/CNT 3% nanocomposite as our model material to improve its processability and reduce its melt viscosity.

The CNT/GNP hybrid filler nanocomposites include 3 % of CNT and different contents of GNP: 0.25, 0.5, 0.75 and 1%. Therefore, the total filler contents were 3.25, 3.5, 3.75 and 4 %.

Morphology

The dispersion of the carbon nanofillers in the PA66 matrix was observed by field emission scanning electron microscopy (FE-SEM). Figure 1 shows selected SEM images of GNP binary nanocomposites and CNT/GNP hybrid filler nanocomposites, both with 0.5 % of GNP-25. The GNP-25 system was chosen because of the larger particle size. It was difficult to differentiate between GNP-2 and CNT nanoparticles in GNP-2 systems (results

no shown). It can be seen GNP and an isolated graphene nanoplatelet in the GNP-25 binary nanocomposites (see Figure 1a black circles). The size of the GNP is well below the original size of 25 μm, which might be an indication of the shear action of the mixing process over the nanoparticles. In Figure 1b, it can be seen both GNP and CNT nanoparticles coexisting in the PA66/CNT 3%/GNP-25 0.5 % nanocomposite. However, the big particle size difference between both nanoparticles makes it difficult to identify both of them in the same zoom scale. In Figure 1b, top, two GNP nanoparticles seem to be spotted (black circles). A zoom image of the area revealed what appear to be an isolate GNP (black circle in Figure 1b, middle). In addition, the bright dots spread in the matrix corresponded to the CNT. It seems that the CNT are well dispersed and not important agglomerates of large size were observed (see Figure 1b, central). Further zooming in allows exposing clearly the CNT (see Figure 1b, bottom, black arrows).

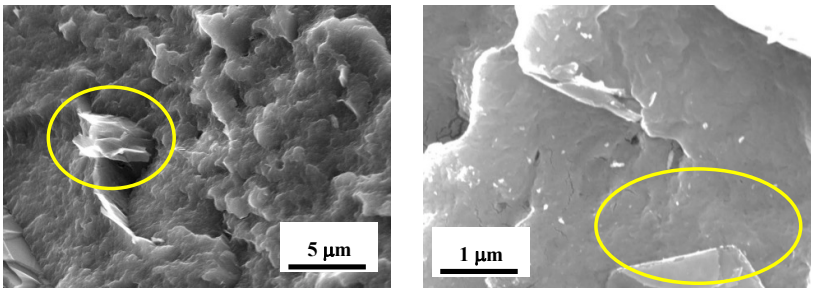

(a)

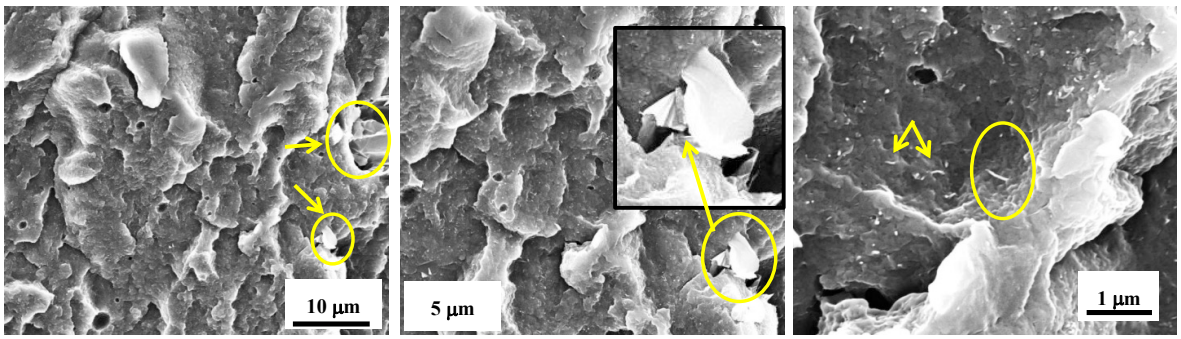

(b)

Figure 1 Scanning electron microscopy images of a) PA66/GNP-25 1% and b) PA66/CNT 3%/GNP-25 0.5 %. Different zoom images.

The SEM images of the cryo fractures revealed that in general, the CNT nanoparticles seems to be well dispersed and homogeneously distributed in the hybrid filler nanocomposites. No presence of agglomerates has been observed. That should guarantee some interactions between the CNT and the GNP nanoparticles.

Rheology

The rheological evaluation in the linear regime allows obtaining information of the viscoelastic response in the melt of the material. First of all, Figure 2a shows the variation of storage module (*G'*) as function of the angular frequency of pure PA66, CNT and GNP binary nanocomposites, and the CNT/GNP hybrid filler nanocomposites with GNP-25 and 3 % of CNT. The pure PA66 exhibited flow behavior in the studied frequency range, with a storage modulus lower than the loss modulus, which means no restriction to flow of the PA66 chains. However, at low frequencies, a plateau in the *G'* value is observed, and the slope deviate from the theoretical relaxation (i.e. $G' \approx \omega^2$). This non-terminal behavior in pure PA66 has been reported earlier[41] and it has been attributed to polymer polydispersity[26,30] or possible post-polymerization process in PA [42].

The oscillatory rheological measurements are suitable for detecting the formation of a percolated network by the nanofillers. As expected, the addition of the nanoparticles promotes a solid-like or non-terminal behavior at low frequencies, below 10^0 rad s^{-1}. This behavior is evident for the CNT binary nanocomposite with 3 % of CNT and the plateau became larger after increasing the CNT content in the CNT binary nanocomposites (4 %)

Comparing the CNT and GNP-25 binary nanocomposites, both with the same content of nanofiller (4 %), it is clear that the GNP is able to modify the elastic response but in lesser extent. A small change in the slope of *G'* can be observed, but the *G'* value is significantly lower than that of the CNT binary nanocomposite. Due to their 1D rod-shape, the CNT nanoparticles are able to create a strong interconnected network that restricted the segmental motions of the polymer chains, increasing the elastic response. On the contrary, the sheet-like geometry of the GNP makes more difficult particle-particle interactions, promoting the slipping between the particles and allowing molecular motions near the interphases[11,12].

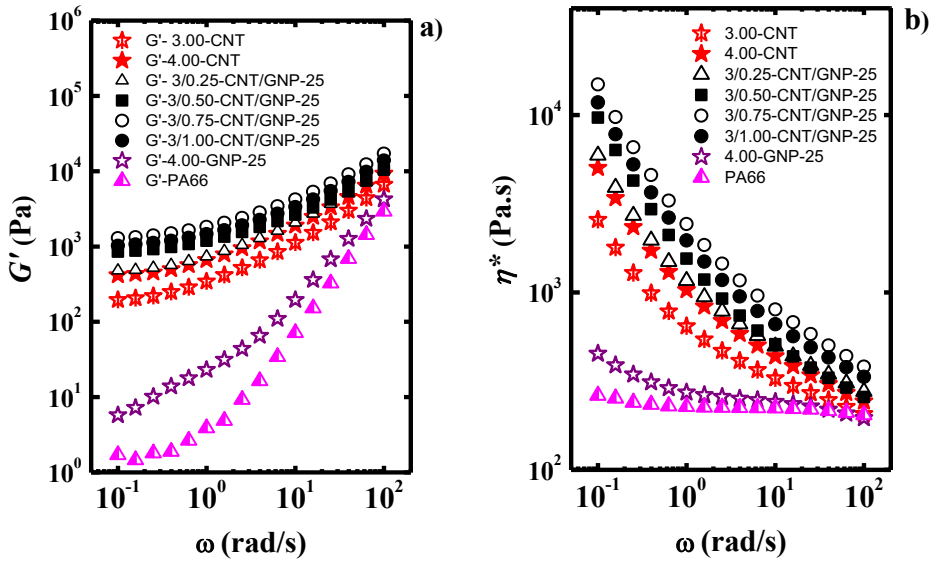

Figure 2 Variation of (a) storage module and (b) complex viscosity as function of the angular frequency of PA66, CNT and GNP nanocomposites, and the CNT/GNP hybrid filler nanocomposites with 3 % of CNT and different content of GNP-25.

The simultaneous addition of both 1-D CNT and 2-D GNP carbon nanoparticles greatly influenced the rheological properties of the nanocomposites. The percolation of the system was confirmed when GNP are included in the formulation. All CNT/GNP hybrid nanocomposites preserved the percolation observed in CNT binary nanocomposites (see *G'* and *G"* plotted together as a function of frequency in Figure S3 in supplementary information). A crossover between *G'* and *G"* was observed in all compositions, and this crossover point took place at higher frequencies for GNP-25 content beyond 0.5%. The stabilization of the *G'* value at low frequencies, in a way that the *G'* is higher than *G"* indicates a transition from a liquid-like to a solid-like response that implies the formation of percolated network created by the nanofillers. If the nanoparticles are very well dispersed and distributed they will create an interconnected network that prevents the flow of the polymers chains around then. Thus, the melt system behaves as a solid rather than as a liquid. The existence of percolated network is required in order to guarantee a good electrical performance. It seems that the GNP-25 presence did not disturb in a great manner the network

created by CNT, and a percolated system prevailed. These observations will reflect on the viscosity of these materials.

Figure 2b shows the complex viscosity of pure PA66, CNT and GNP binary nanocomposites, and the CNT/GNP hybrid nanocomposites with GNP-25 and 3 % of CNT. The pure PA66 exhibited a Newtonian behavior in which the viscosity is almost independent of frequency. As expected, the addition of 3% of CNT (our model nanocomposite) highly increased the viscosity of the PA66. This increment was even higher when content of CNT is increased up to 4%. The nanoparticles restrict the molecular motions of the polymer chains near the interphase, leading to an increment of the viscosity. On the contrary, the addition of 4% of GNP-25 increased the viscosity of the PA66 matrix but in a lesser extent. These observations have been reported previously[11] and were as expected. However, the simultaneous addition of both CNT and GNP does not seem to improve the flow properties of the PA. In general, the CNT/GNP hybrid nanocomposites exhibited higher viscosities than the CNT binary nanocomposites, regardless the GNP-25 content. The tendency with GNP-25 composition was not clear since the highest GNP-25 content in the PA66/CNT nanocomposite (3/1-CNT/GNP-25) exhibited slightly reduced viscosity. This unexpected behavior might be related with some agglomeration of the bigger GNP-25 particles that could impoverishing their appropriate dispersion and interaction with the particle network. Despite that fact, the 3/1-CNT/GNP hybrid nanocomposite exhibited even higher viscosity than that of the analogous CNT binary nanocomposite with the same total filler content of 4%.

Since no reduction in the nanocomposite viscosity was obtained after the addition of GNP of 25 μm, another graphene with smaller particle size (2 μm) and higher specific surface area (750 m^2 g^{-1}) was evaluated for comparison purposes. The GNP-2 has a surface area which is 5 times higher than that of the GNP-25 and this characteristic, along with the smaller particle size, may modify the rheological response of the system. Figure 3a shows the variation of storage module (*G'*) as function of the angular frequency of pure PA66, CNT and GNP binary nanocomposites, and the CNT/GNP hybrid filler nanocomposites with GNP-2 and 3 % of CNT. The GNP-2 binary nanocomposite followed the same trend than the GNP-25 one. A small change in the slope of *G'* was observed at low frequencies. However, a different trend was observed in the CNT/GNP-2 hybrid filler nanocomposites. There is no

clear tendency with composition. Interestingly, increasing the GNP-2 content up to 1 % led to an important reduction of the storage modulus (see 3/1.00-CNT/GNP-2).

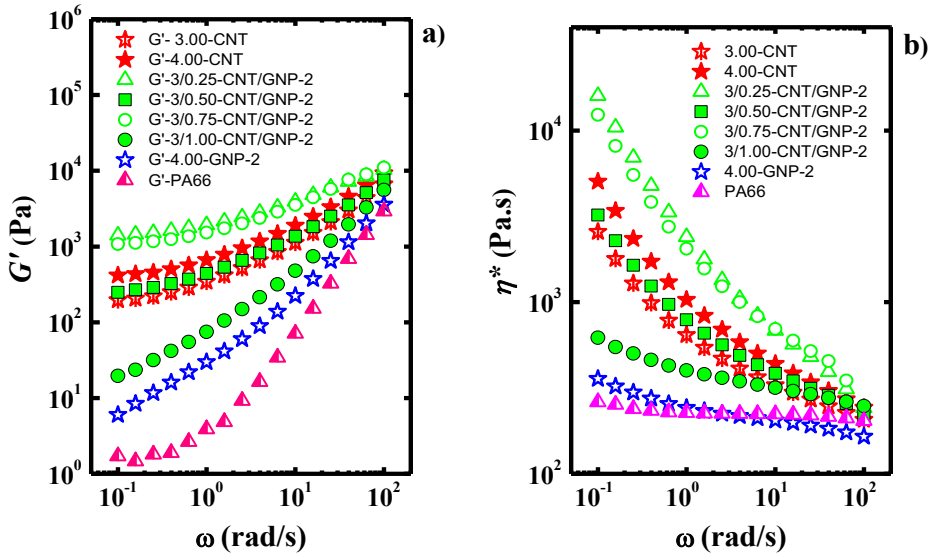

Figure 3 Variation of (a) storage module and (b) complex viscosity as function of the angular frequency of PA66, CNT and GNP nanocomposites, and the CNT/GNP hybrid nanocomposites with 3 % of CNT and different content of GNP-2.

The presence of a percolated network was also verified in the CNT/GNP-2 hybrid filler nanocomposites (see *G'* and *G"* plotted together as a function of frequency in Figure S4 in supplementary information). The introduction of GNP of smaller particle size did modify the percolated network created by the CNT. At higher GNP-2 content (1 %), no percolation (crossover between *G'* and *G"*) was observed in the range of frequencies evaluated. This aspect will be further discussed in the next section.

Similar to *G'* tendency, the effect of GNP-2 on viscosity is not clear (see Figure 3b). However, including 1 % of GNP-2 drastically reduced the melt viscosity, in comparison to the CNT binary nanocomposites. We cannot provide an explanation for the unclear tendency observed. It is possible that a high content of well-dispersed GNP-2 nanoparticles with high surface area might have induced more interactions with the polymer matrix in which the CNT are embed causing disruption of the CNT network and promoting the flow of the polymer chains. Despite that, it seems that the graphene size did influence the rheological behavior of

the hybrid nanocomposites. Therefore, the following figures display selected results to better understand the effect of the GNP size in the rheological properties.

Figure 4a,b compared the storage modulus of the CNT/GNP hybrid nanocomposites with different graphene size and content. First of all, it is clear that the addition of both CNT and GNP increased the *G'* value of the PA6 matrix. When the high size GNP is used, not major difference is observed with composition. However, the hybrid nanocomposites with GNP-2 exhibited lower storage modulus. Moreover, increasing the GNP-2 content further decreased the elastic response of the system. The viscosity values followed the same trend (see Figure 4c,d). The CNT/GNP hybrid nanocomposite with the lowest viscosity is the one with highest content of GNP-2, which is the graphene of smaller particle size.

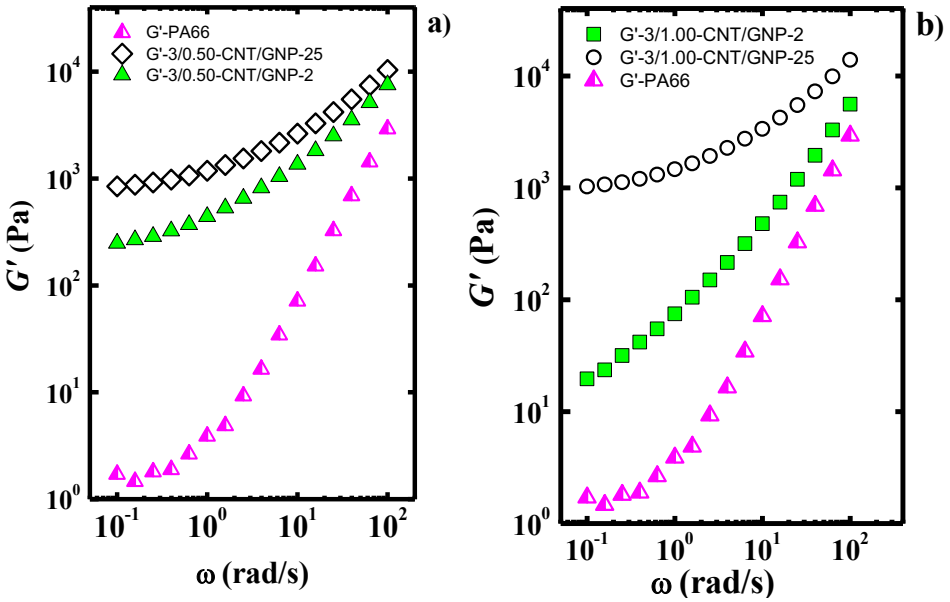

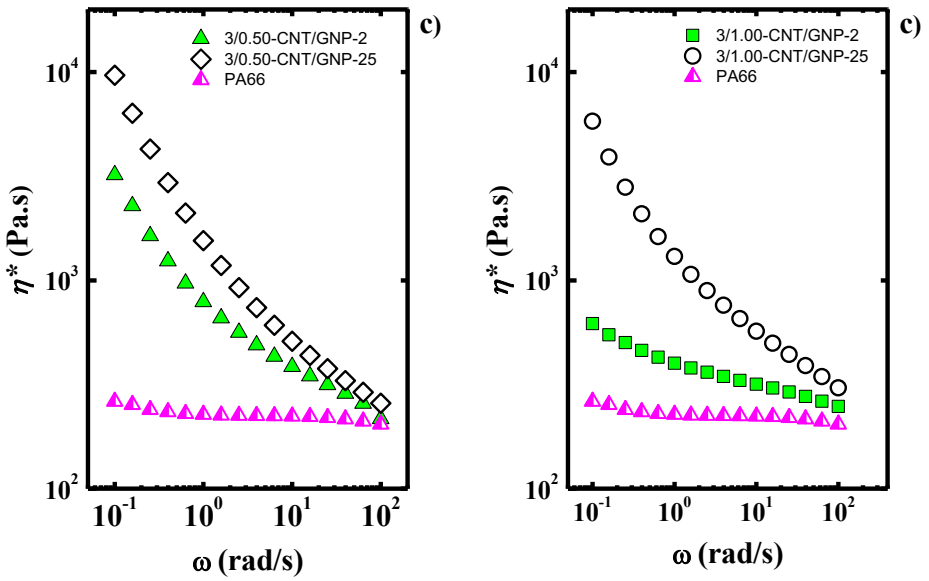

Figure 4 Variation of storage module (*G'*) and complex viscosity (η*) as function of the angular frequency of PA66, and the CNT/GNP hybrid nanocomposites with 3 % of CNT and a,c) 0.5 % or b,d) 1 % of GNP-25 and GNP-2.

Since the CNT/GNP hybrid nanocomposite with 1 % of GNP-2 exhibited the lowest viscosity, the following pictures compare the rheological behavior of pure PA66, CNT and GNP binary nanocomposites, and CNT/GNP hybrid nanocomposite with 3% of CNT and 1 % of GNP-25 or GNP-2. Figure 5 shows the variation of storage module (*G'*) as function of the angular frequency of the aforementioned systems.

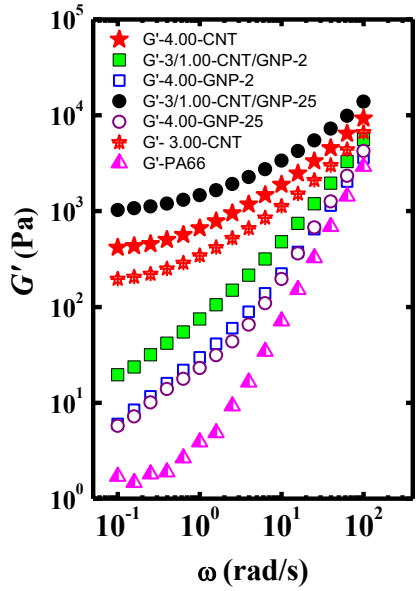

Figure 5 Variation of storage module (*G'*) as function of the angular frequency of pure PA66, CNT and GNP binary nanocomposites, and the CNT/GNP hybrid filler nanocomposites with 3 % of CNT and 1 % of GNP-25 or GNP-2.

The addition of 4 % of GNP to the PA66 polymeric matrix increased the *G'* value. It is clear that the GNP nanoparticles modify in some extend the elastic response of the system. However, it seems that the effect of graphene size was not significant enough to influence the storage modulus, at least at this composition (4 %). On the contrary, the addition of CNT highly increased the *G'* values in the CNT binary nanocomposites. In fact, the storage modulus increased as the CNT content is higher and, it is greater than the storage modulus of the GNP binary nanocomposites with same nanofiller content (4 %). In addition, the CNT nanocomposites exhibited a clear solid-like behavior at low frequencies, expected in highly-loaded nanocomposites. This solid response is an evidence of the presence of a percolated network. The CNT/GNP hybrid filler nanocomposites with GNP-25 and GNP-2 exhibited an interesting behavior. In these hybrid nanocomposites, the content of CNT and GNP is 3 and 1 %, respectively. Therefore, the total nanofiller content is also 4 %. When the GNP-25 is used, the *G'* value is higher than analogous CNT binary nanocomposite with 3 % of nanofiller, probably due to the higher total nanofiller content resulted from the addition of the GNP-25. However, the *G'* value is even higher to that of the analogous CNT binary nanocomposite with the same nanofiller content. A clear solid-like response is exhibited at

low frequencies. This behavior is strictly related with the formation of the percolated network by both nanofillers. On the contrary, the addition of 1 % of the graphene of smaller size, that is the GNP-2, provided an intermediate behavior. The *G'* values are higher than those of the GNP binary nanocomposites but lower than those of the CNT binary composites and the hybrid one with GNP-25. In addition, no plateau is observed in the *G'* variation with frequency. Thus, no solid-like behavior was exhibited. Further evidence of the formation (or not) of a percolated network is given in Figure 6.

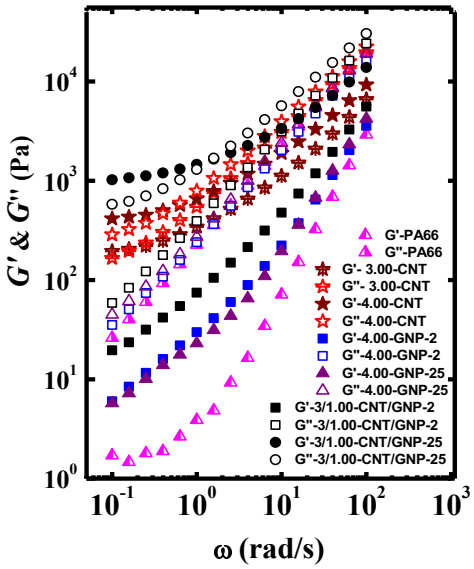

Figure 6 Variation of storage (*G'*) and loss modules (*G''*) as function of pure PA66, CNT and GNP binary nanocomposites, and the CNT/GNP hybrid filler nanocomposites with 3 % of CNT and 1 % of GNP-25 or GNP-2.

Plotting *G'* and *G"* together allows to identify the formation of a percolated network in the range of frequencies and compositions evaluated. Figure 6 shows the variation of *G'* and *G''* as a function of frequency of pure PA66, CNT and GNP binary nanocomposites, and the CNT/GNP hybrid filler nanocomposites with 3 % of CNT and 1 % of GNP-25 or GNP-2. As expected, the absence of a crossover between *G'* and *G"* for pure PA6 is clear, since no restriction is imposed to the segmental motions of the polymer chains. A crossover of *G'* and *G"* indicates a transition from a liquid-like to a solid-like behavior. The elastic response becomes more important than the viscous one due to the formation of a percolated network structure created by the nanofillers. From Figure 6, it can be seen that no percolation is

observed in both GNP binary nancomposites with 4 % of nanofiller. On the contrary, both CNT binary nanocomposites with 3 and 4 % of nanofiller exhibited a crossover between *G'* and *G''* at frequencies beyond 10^{-1} rad s^{-1}. That is a clear evidence of the formation of a percolated network through interactions between the nanofillers and with the polymer chains. These interactions will hinder the segmental motions of the polymer chains at the interphase, preventing their flow. The differences between CNT and GNP nanocomposites obeyed the differences in geometry and aspect ratio of the nanofillers. The 1-D geometry and high aspect ratio of the CNT allow them to interconnect to create a network. On the contrary, the sheet-like structure of the graphene nanoplatelets makes them more difficult to disperse and creates particle-particle interactions, and therefore, higher GNP content is needed. Similar results have been reported before by Xiao et al.[4] in PVDF/GNP nanocomposites. A very high GNP content, up to 20 %, was required to observe a clear solid-like behavior. Mayoral et al.[25] have reported a rheological percolation at 10 % and 15 % of GNP in PA6/GNP nanocomposites. In our case, the 4 % of GNP was not sufficient to promote the formation of a percolated network.

In the case of the hybrid nanocomposites, two opposite behaviors were observed. The addition of GNP-25 preserved the network created by the CNT, shifting the percolation crossover to even higher frequencies. On the contrary, the CNT/GNP hybrid nanocomposite with the GNP of smaller particle size (GNP-2) did not exhibit a crossover in the range of frequencies evaluated. In other words, the addition of GNP-2 disturbed the percolated network created by the CNT. The two behaviors might be related to the GNP particle size. Since CNT and GNP are carbon nanofillers, it is expected that they will interact through π-π interactions, enhancing the percolation. In fact, some authors propose that the CNT could form bridges that interconnect the graphene nanosheets [1], improving the percolation of the network. This GNP-CNT network might confine the polymer chains inside, preventing their flow. That might be a reason why the CNT/GNP hybrid nanocomposite with GNP-25 exhibited the highest percolation and storage modulus.

In comparison to the GNP-25, the GNP-2 has lower particle size and higher specific surface area (750 vs 120-150 m^2 g^{-1}). These features might contribute to a better dispersion of the nanosheets in the polymer matrix. The nanoflakes might slip through the polymer interphase, interrupting the connections between the nanotubes, and therefore, disrupting or

hindering the formation of the finer CNT network. The CNT might be trapped in between the nanosheets of graphene due to their different aspect ratio and size.

Similar rheological behavior has been reported by Xiao et al.[4] and Doagou-Rad et al.[31] in binary and hybrid filler PVDF and PA66 nanocomposites, respectively. The storage modulus of binary PVDF/GNP nanocomposites remained similar for GNP compositions between 1 and 5%, and increased with 10 % of GNP. However, the *G'* values are still lower than of the PVDF/CNT binary nanocomposite with 2 % CNT. It only started to become frequency independent at very high GNP content. Similar to our hybrid nanocomposites with GNP-25, the PVDF/CNT/GNP hybrid nanocomposites exhibited a solid-like behavior with only 1% of GNP, and the response became more pronounced as the content of GNP increased. The other rheological properties (η^*, *G"*) followed the same trend. It is worth mentioning that the size of the GNP used was 5-7 μm. It is possible that only very small GNP, as our 1-2 μm size GNP-2, are able to modify the percolated behavior that is already exhibited by the CNT binary nanocomposites.

The intermediate rheological behavior of our CNT/GNP hybrid nanocomposite with GNP-2 was also reported by Doagou-Rad et al.[31] Unlike the present study, the authors employed GNP of smaller size: 30 nm-1μm. Their CNT/GNP hybrid filler nanocomposites exhibited higher storage modulus than GNP nanocomposites but lower than that of the CNT ones. Contrary to our results, the authors claimed that the $\tan \delta = G''/G'$ values were less than one through the whole span of the studied frequencies, indicating the dominance of a solid-like behavior of the melt, although the results were not presented [31]. No further insight in the rheological behavior is presented by the authors.

The effect of adding GNP nanofillers is also observed in the viscosity of the systems. Figure 7 shows the variation of complex viscosity (η^*) as function of the angular frequency of PA66, CNT and GNP binary nanocomposites, and the CNT/GNP hybrid filler nanocomposites with 3 % of CNT and 1 % of GNP-25 or GNP-2.

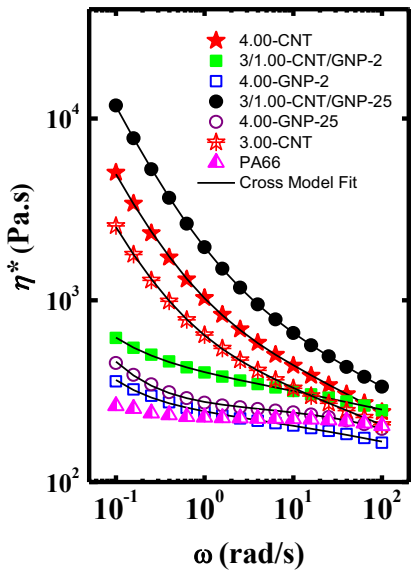

Figure 7 Variation of complex viscosity (η*) as function of the angular frequency of PA66, CNT and GNP binary nanocomposites, and the CNT/GNP hybrid filler nanocomposites with 3 % of CNT and 1 % of GNP-25 or GNP-2. The lines corresponded to the Cross Model fitting

In all the nanocomposites, it can be seen that the addition of the nanofillers caused an augmentation of the viscosity at lower frequencies. As aforementioned, the CNT binary nanocomposites exhibited a higher viscosity than the GNP binary ones, mostly due to the difference in the geometry and aspect ratio between both nanoparticles explained before. The addition 1% of GNP-25 in the CNT/GNP hybrid nanocomposites did not decrease the viscosity of the system. However, it is clear that employing a graphene of smaller particle size (GNP-2: 2 μm) drastically reduced the viscosity of the hybrid nanocomposite. Due to their higher interfacial surface and lower size, the graphene nanoplatelets might allow the movement of the polymer chains near the interphase and across the CNT network, through a slipping effect favored by their 2-D geometry [11]. In addition, it has been reported a lubricating effect associated to GNP platelets[15] that can contribute to the flow of the system as the size of the GNP decreases (higher aspect ratio and superficial area). In fact, no significant increment in the viscosity is observed for the binary PA66/GNP nanocomposites, and the viscosity of the PA66/GNP-2 system is lower than that of the PA66/GNP-25 (at same 4 % composition). Therefore, the GNP-2 was successful in reducing the viscosity of CNT nanocomposite through a hybrid filler approach. However, this CNT/GNP hybrid

nanocomposite did not exhibit percolation, and that factor may affect the electrical performance of the system. This will be discussed in the upcoming section regarding the electrical properties.

Finally, the experimental viscosity values were fitted through the Modified Cross Model (see black lines in Figure 7). This model allows fitting the increasing of the viscosity at lower frequencies, which is typically observed in nanocomposites. From the equation 1 presented in the experimental section, 4 parameters can be determined: the zero shear viscosity, η_0, the limiting stress, σ_0, the relaxation time, τ and the pseudoplasticity index, n. In Figure 7 it can be seen that the model adjust perfectly to the experimental results. The r^2 values were higher than 0.9999. The resulting parameters are resumed in Table S1 in the suplemmentary information, and the more relevant are presented in Figure 8 as a function of the total nanofiller content. Additional CNT and GNP compositions were prepared and included in the binary nanocomposites in order to broaden the composition range for comparison purposes.

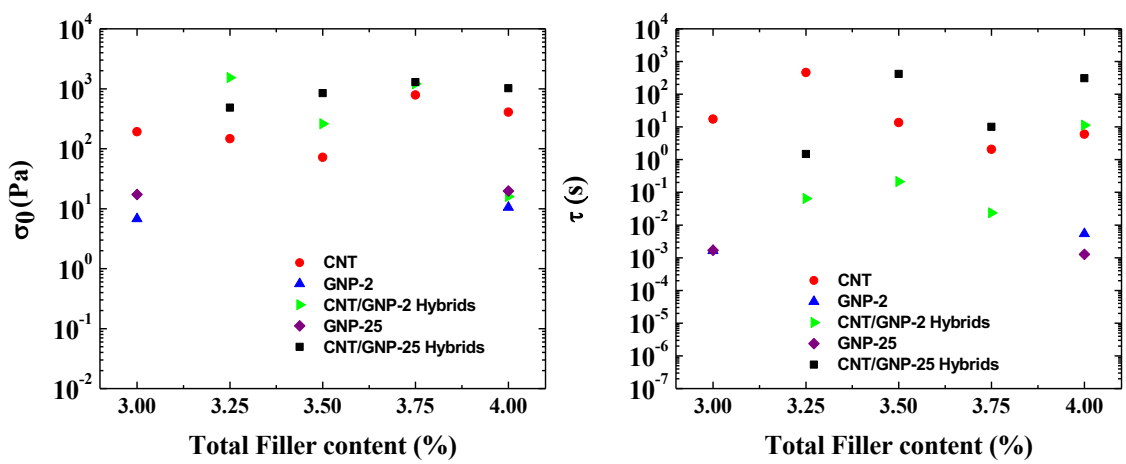

Figure 8 Variation of the yield stress (σ_0) and the relaxation time (τ) as a function of the total nanofiller content for PA66, CNT and GNP binary nanocomposites, and the CNT/GNP hybrid filler nanocomposites with GNP-25 and GNP-2.

The yield stress, σ_0, represents the increment of the viscosity at low frequencies. It gives information about the state of the dispersion [43]. From Figure 8, it can be seen that in the hybrid and CNT nanocomposites, the values are more or less in the same range with

composition. That is probably due to the fact that systems are already high-loaded. It has been reported that the σ_0 values reach a plateau as composition increase [35]. Despite that, the hybrid and CNT nanocomposites exhibited higher yield stress than the GNP binary nanocomposites. Similar tendency has been reported by Martin-Gallego et al., who fitted their experimental data to the Herschel–Bulkley model, from which the yield stress value can also be determined. A good correlation of the model to the experimental data was reported by the authors [11]. A representation of the yield stress can be also observed in Figure 9, in which the viscosity is plotted versus the torque applied. The viscosity tends asymptotically to infinite at a certain value of torque. That will indicate the presence of a yield stress [11]. It can be seen that the appearance of the yield stress took place for the CNT nanocomposites and CNT/GNP-25 nanocomposite. That indicates an increment of the viscosity at low frequency values as it was observed in Figure 7. On the contrary, a yield stress did not emerge for the GNP nanocomposites and CNT/GNP-2 nanocomposite revealing a more liquid like behavior and a reduced viscosity, as a consequence of less interconnection between the nanoparticles.

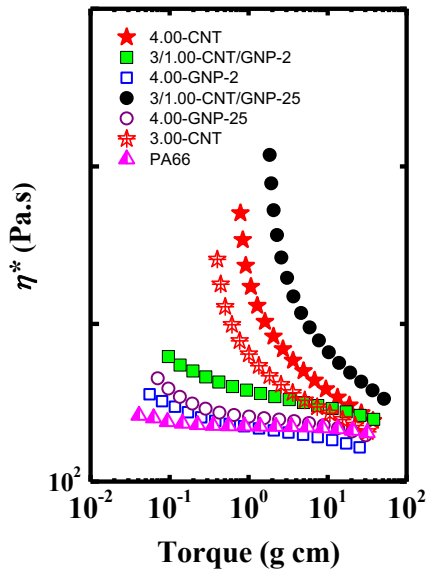

Figure 9 Variation of complex viscosity (η*) as function of the torque of PA66, CNT and GNP binary nanocomposites, and the CNT/GNP hybrid filler nanocomposites with 3 % of CNT and 1 % of GNP-25 or GNP-2.

Interesting are the result of the relaxation times (τ). The value of τ represents the time the polymer chains take to relax completely while they are melt processed.[13] Although, the tendency is not very clear with composition, it seems that the relaxations are faster in the GNP binary nanocomposites, and slower in the CNT binary and CNT/GNP hybrid filler nanocomposite with GNP-25. Faster relaxations would indicate a more liquid-like response while slower relaxations would agree with a solid-like behavior, which agree well with the *G'* and *G"* behavior that was observed and already discussed for these systems. Higher relaxation times indicate a hinder of the polymer chains mobility due to the presence of a percolated network structure created by the nanofillers, and therefore requires longer times in order to break the interconnections.[13]

Further evidence of the characteristic time is given in Figure 10. It can be seen that the *tan* δ peak shifted to higher frequencies and becomes broader, as previously reported in polymer nanocomposites. In addition, below frequencies of 10^0, the *tan* δ values of the PA66/CNT nanocomposites (open and closed red stars) and the hybrid nanocomposite with GNP-25 (black circles) became less than 1, indicating the transition to a solid like behavior. This rheological behavior has also been reported by Nunes et al.[13] in blends of PE/ poly(ethylene-co-methyl acrylate) with both CNT and GNP included. The authors found that the PE and blends with GNP only exhibited *tan* δ values > 1, indicating a more liquid like behavior (as in our PA66/GNP nanocomposites, open purple circles and blue squares), while the PE blends with only CNT and both CNT and GNP exhibited *tan* δ values < 1, suggesting that the network of CNT is better developed in blends. Similarly, the authors also reported longer relaxation tines for the blends with CNT and CNT/GNP, in comparison to the composites with GNP only.

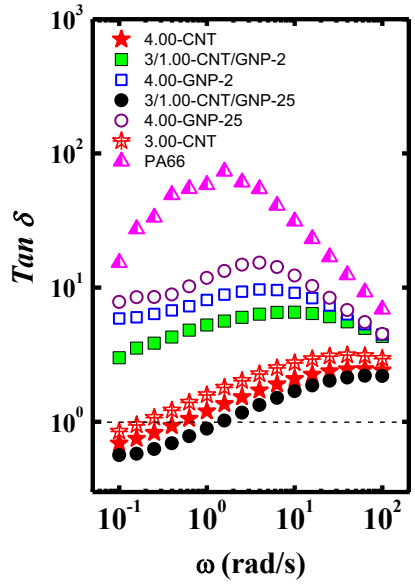

Figure 10 Variation of *tan δ* peak as function of angular frequency of PA66, CNT and GNP binary nanocomposites, and the CNT/GNP hybrid filler nanocomposites with 3 % of CNT and 1 % of GNP-25 or GNP-2.

Electrical properties

The rheological performance is strictly related to the final electrical performance of the systems. A well percolated network, created by the nanofillers, is required in order to properly conduct the electrons through the polymer matrix. Figure 11 shows complementary electrical conductivity (σ) evaluations of the CNT and GNP binary nanocomposites, and the CNT/GNP hybrid filler nanocomposites with GNP-25 and GNP-2, as a function of viscosity of the systems.

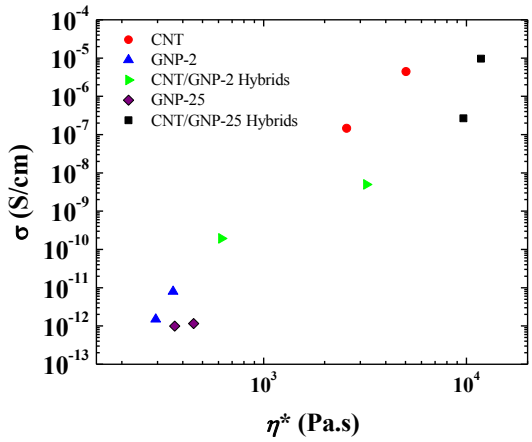

Figure 11 Electrical conductivity as a function of viscosity at 10^{-1} rad/s, of the CNT and GNP binary nanocomposites, and the CNT/GNP hybrid filler nanocomposites with GNP-25 and GNP-2.

It can be seen that the CNT binary nanocomposites (red circles) exhibited higher electrical conductivity than the analogous GNP ones (blue triangles and purple diamonds). The CNT/GNP hybrid nanocomposites (green triangles and black squares) exhibited intermediate values of electrical conductivity and viscosity. Similar intermediate values has been reported by Prolongo et al.[1] in epoxy/CNT/GNP nanocomposites, Rostami et al.[14] in PP/CNT/GNP nanocomposites and Feng et al.[16] in PE/CNT/Boron nitride nanocomposites. Particularly, Rostami et al.[14] reported that the electrical resistivity of the hybrids was higher than that of the PP/CNT nanocomposite but the values fallen below the mixture law, indicating the formation of an efficient continuous interconnecting network. Similarly, a reduction of the electrical conductivity was observed by Feng et al.[16] with the addition of both CNT and boron nitride particles, if comparisons are made with PE/CNT binary system. However, in this last case, the reason behind the reduced conductivity is the electrical insulating nature of the boron nitride particles.

In the present work, the conductivity values of the CNT binary nanocomposites and the CNT/GNP-25 hybrid filler nanocomposites were between 10^{-7} and 10^{-5} S/cm, while the GNP binary nanocomposites exhibited very low conductivities, around 10^{-12} S/cm. The conductivity values reported in the literature for PA6/CNT nanocomposites are very wide, ranging from 10^{-15} to 10^{-3} depending on CNT composition[33,44-46]. With 3 % of CNT, it has

been reported conductivities of 10^{-14} [33], 10^{-12} [45] and 10^{-4} [46] S/cm. And electrical percolation thresholds are reported at 1.5 [28] 2.5 [44], and 4% [33]. The differences might be due to mixing conditions and functionalization treatments. In the case PA6/GNP nanocomposites, the values vary between 10^{-14} and 10^{-3} [25,47], with percolation thresholds at 10 % [25]. With 3 % of GNP, values between 10^{-13} and 10^{-12} S/cm have been reported [25]. Those values agreed well with our results. It has been reported that the rod like structure of the CNT is more effective in creating conducting networks than the sheet like form of the GNP platelets.[13] In addition, the intrinsic electrical conductivity of the nanoparticles may have an influence on the electrical behavior obtained. The electrical conductivity of graphene is different in the 2D plane in comparison to across their thickness, unlike the carbon nanotubes that can exhibit unidirectional electrical conductivity along the tube. In the GNP used in this work, the electrical conductivity in the parallel direction to surface is 10^7 S/m while in the perpendicular direction is 10^2 S/m.

In order to conduct electricity, a very well percolated network created by the nanofillers is required. The rheological measurements demonstrated the formation of a percolated network by the CNT. According to the rheological results, those systems with a clear sign of percolation exhibited higher electrical conductivity values (CNT binary nanocomposite (red circles) and CNT/GNP-25 hybrid filler nanocomposite (black squares)). On the contrary, the GNP binary nanocomposite (blue triangles and purple diamonds) and the CNT/GNP-2 hybrid filler one (green triangles) exhibited lower values. It seems that lower size GNP-2 disrupted the well percolated network created by the CNT, impoverishing the electrical performance. Both Araby et al.[3] y Xiao et al.[4] reported that the addition of CNT to EPDM/GNP and PVDF/GNP nanocomposites enhanced the electrical performance of the system. This improvement demonstrated that the CNT nanoparticles are the main responsible for the conductance of the electricity through the polymer matrix. However, the addition of CNT increases the viscosity of the systems. Figure 11 demonstrated that intermediate properties of reduced viscosity and improved electrical conductivity are achieved when GNP-2 (lower particle size graphene) and CNT are combined. As the CNT percolated network contributes to provide electrical conductivity to the polymeric matrix, the GNP induces a reduction of the high viscosity caused by CNT presence through a disruption of the

fine CNT network in such extend that some electrical conductivity is retained. Ultimately, exists a compromise between a reduced viscosity while holding electrical conductivity. Thus, the CNT/GNP-2 hybrid filler nanocomposites (green triangles) exhibited the best balance of properties pursued.

Non-isothermal crystallization behavior of selected systems

Complementary crystallization behavior study of the systems was performed. The non-isothermal crystallization behavior of selected systems was evaluated by differential scanning calorimetry (DSC). The characteristic thermal properties obtained during heating and cooling scans are presented in Table 3.

Table 3 Thermal properties of PA66 in nanocomposites obtained from DSC cooling and heating scan

System	Samples	T_c PA66 (°C)	ΔH_c PA66 (J/g)	T_m PA66 (°C)	ΔH_m PA66 (J/g)	χ_c (%)
Pure PA	PA66	231.1	63	262.0	74	39
Carbon nanotubes nanocomposites	3.00-CNT	241.9	74	260.9	86	45
	4-CNT	241.3	75	262.0	81	43
Graphene nanocomposites	3.00-GNP-2	239.5	61	261.9	75	39
	4.00-GNP-2	239.7	60	262.3	72	38
Hybrid filler nanocomposites:	3/0.50-CNT/GNP-2	242.3	77	260.4	88	47
	3/1.00-CNT/GNP-2	241.6	73	260.8	85	45

From results presented in Table 3 it is clear that the addition of either CNT, GNP or hybrid filler enhance the crystallization behavior of the PA66 matrix. The crystallization temperature (T_c) increased between 8 and 10 °C, in comparison to the pure PA66, regardless type of carbon nanofiller present in the nanocomposite. This observation has been well reported in polymer nanocomposites. The increment in T_c is the result of a nucleating effect induced by the nanofillers, which could act as nucleating agents for PA66. Despite the improved crystallization temperature, the crystallization degree (χ_c) did not changed significantly, since the values are within the experimental error of the measurements. Similar results have been reported by Xiang et al.[20], Doagou-Rad et al.[31], and Sreekanth et al.[32] Moreover, the melting point values do not significantly vary in comparison to that of pure PA66.

Determination of the nucleation efficiency

It is well known that nanoparticles can enhance the crystallization behavior of semicrystalline polymers. Most of them play a role as nucleating agents, increasing the melt-crystallization temperature. That is the common behavior reported in the literature. However, most reports do not provide evidence of the quality of the nanoparticles as nucleating agents. In order to do that, a proper study of Self-Nucleation of the pure thermoplastic matrix needs to be conducted. After that, the nucleation efficiency of the carbon nanoparticles can be provided. Only few publications have reported the nucleation efficiency of the carbon nanoparticles such as carbon nanotubes in thermoplastic matrices[48].

The self-nucleation experiments allow determining the *ideal self-nucleation temperature* T_s, which is the lowest temperature (without annealing) at which a polymer can crystallize from nuclei of its own. In this way, the nucleating effect caused by the own nuclei of the polymer is compared to the effect caused by the carbon nanoparticles. Similar to the present study, a self-nucleation analysis have been reported by Xiang et al.[20] in PA6/ reduced graphene oxide nanocomposites. However, the analysis was conducted in order to evaluate the crystallization kinetics of the system taking into account the nucleation and crystal growth contributions, and no mention was made of the nucleation efficiency.

Thus, the self-nucleation experiment was applied here to the pure PA66, following the procedure described in the Experimental Part, in order to determine the self-nucleation domains and the *ideal self-nucleation temperature* T_s. Figure 12 shows the cooling scans from the indicated T_s and the subsequent heating scans.

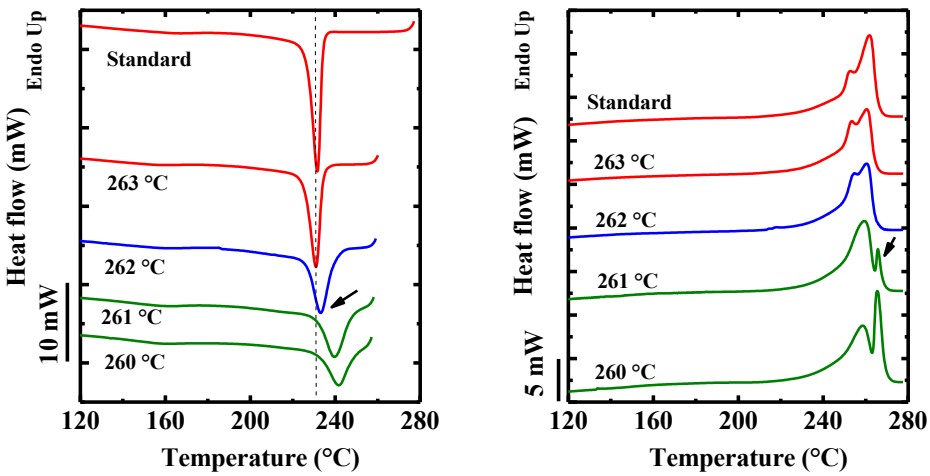

Figure 12 Self-nucleation of PA66. DSC cooling scans from indicated T_s values (left) and subsequent DSC heating scans (right) (A color code has been employed to indicate the self-nucleation domains: red for *Domain I*, blue for *Domain II* and green for *Domain III*)

At higher T_s values, the DSC cooling scans remained the same (the crystallization of PA66 took place at the same temperature (red curves in Figure 12, left)), but as the T_s temperature was decreased until 262 ºC, the crystallization peak shifted to higher values (see blue curve in Figure 12, left), while not change is observed in the subsequent heating scan (see blue curve in Figure 12, right). That indicated the transition from *Domain I* to *Domain II*. At 262 ºC, the self-nucleation domain took place, which means that at this temperature the PA66 droplets have been injected with enough self-nuclei that enhanced its crystallization. As the T_s values were further reduced, an increase in the PA66 crystallization temperature was obtained, as expected.

The transition from *Domain II* to *Domain III* occurred at 261 ºC, a temperature in which a second melting peak appeared in the subsequent heating scan (indicated with an arrow in the green curve of Figure 12, right). This higher temperature endothermic peak corresponds to the melting of the annealed crystals at T_s equal to 261 °C and below.

A representation of the three domains of self-nucleation is presented in Figure 13. A standard DSC melting curve is plotted employing the same color code to indicate the determined self-nucleation domains: red for *Domain I*, blue for *Domain II* and green for *Domain III*. The domain transitions are marked by vertical lines. On top of the DSC heating trace, the variation of peak crystallization temperatures T_c as a function of T_s values is plotted.

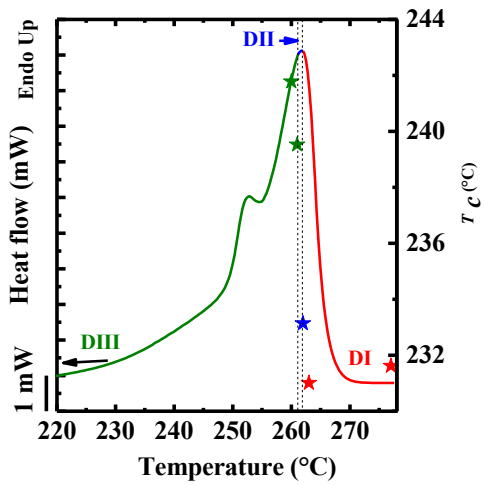

Figure 13 Representation of the self-nucleation domains for PA66 on top of the standard DSC melting trace. The data points represent peak crystallization temperatures (plotted on the left-hand side y axis) as a function of T_s values.

The domain window of exclusive self-nucleation (*Domain II*) is very narrow (only 1 degree, blue star) and the self-nuclei are most probably made of crystal fragments, since most of the domain covers the tail of the melting peak[39]. In the transition to *Domain III* the T_c values continue to increase.

From the above analysis, the *ideal self-nucleation temperature* T_s of PA66 was 262 °C. It is an ideal temperature because it is the lowest temperature at with the PA66 can be self-nucleated without annealing. After self-nucleating at this temperature, the maximum crystallization temperature of PA66 was 233.1 °C (blue star in Figure 13). This value was used to compare the crystallization ability of selected binary and hybrid nanocomposites, in the presence of the nanofillers. By equation 4 [48], the nucleation efficiency (*NE*) of the CNT, GNP and the CNT/GNP hybrid can be determined:

$$NE = \frac{T_{C,NA} - T_{C,PA66}}{T_{cmax} - T_{c,PA66}} x100 \qquad eq.4$$

where $T_{c\,NA}$ is the peak crystallization temperature of the polymer with the nucleating agent (in this case CNT, GNP or hybrid filler), $T_{c,PA66}$ is the peak crystallization temperature of neat PA66 after erasing its crystalline history (231.1 °C) and $T_{c,max}$ is the maximum crystallization

temperature after PA66 has been self-nucleated at the ideal self-nucleation temperature (233.1 °C). The nucleation efficiency of selected systems is reported in the following table.

Table 4 CNT, GNP and hybrid filler efficiency as nucleating agents

System	Samples	T_c PA66 (°C)	Nucleation efficiency (%)
Carbon nanotubes nanocomposites	3.00-CNT	241.9	522
	4-CNT	241.3	491
Graphene nanocomposites	3.00-GNP-2	239.5	406
	4.00-GNP-2	239.7	414
Hybrid filler nanocomposites:	3/0.50-CNT/GNP-2	242.3	538
	3/1.00-CNT/GNP-2	241.6	507

From Table 4, it is clear the excellent action of CNT and GNT as nucleating agents. Nucleation efficiencies around 500 % were determined, indicating the supernucleating effect of these materials. Therefore, the addition of GNP and CNT contributes to enhance the crystallizability of these materials, in terms that higher crystallization temperatures can be used during molding processing. Similar results have been reported filled with CNT. Trujillo et al.[48] reported a supernucleation effect of CNT in polycaprolactone (PCL) / CNT nanocomposites. The authors reported NE values of 200 %. Supernucleation, ascribed when the nucleation efficiency is greater than 100 %, has also been reported in PE and polyethylene oxide nanocomposites with CNT. Therefore, the addition of the carbon nanofillers to the PA66 will improve the crystallization of PA66, in terms of higher crystallization temperatures.

CONCLUSIONS

In this work, the rheological performance and electrical properties of PA66/CNT/GNP, PA66/CNT and PA66/GNP nanocomposites were evaluated.. The effect of two GNP of different lateral size (25 and 2 μm) and surface area (120-150 and 750 $m^2 g^{-1}$) was addressed. The inclusion of GNP in the formulation (as in the PA66/CNT/GNP nanocomposite) successfully reduced the viscosity of the system. This reduction was even greater when the GNP of smaller particle size (2 μm) was used. However, this fact yielded lower electrical conductivity values, probably due to a disruption of the well-connected CNT network. The fitting of the experimental viscosity values to the Modified Cross Model confirmed that the addition of GNP of smaller particles size might reduce the relaxation time of the polymer matrix, enhancing the ability to flow of the system.Complementary study of the crystallization behavior demonstrated the supernucleating effect of both GNP and CNT nanofillers. Nucleation efficiencies of about 500 % were determined. The increment in the crystallization temperature observed was a consequence of the outstanding role of these carbon nanofillers as nucleating agents.The hybrid filler approach was successful in order to obtain CNT nanocomposites of lower viscosity. Further investigations need to be pursued to adjust the nanofiller composition in order to obtain a good commitment between processability and good electrical performance.

REFERENCES

1. Prolongo SG, Moriche R, Ureña A, Florez S, Gaztelumendi I, Arribas C and Prolongo MG, *J. Appl. Polym. Sci.* **135:** 46475 (2018).
2. Poosala A, Hrimchum K, Aussawasathien D and Pentrakoon D, *J Nanomater* **2015:** 1-9 (2015).
3. Araby S, Saber N, Ma X, Kawashima N, Kang H, Shen H, Zhang L, Xu J, Majewski P and Ma J, *Mater Des (1980-2015)* **65:** 690-699 (2015).
4. Xiao Y-j, Wang W-y, Chen X-j, Lin T, Zhang Y-t, Yang J-h, Wang Y and Zhou Z-w, *Compos Part A Appl Sci Manuf* **90:** 614-625 (2016).
5. Chen H-M, Shao L-N, Shen Y, Yang J-H, Huang T, Zhang N, Wang Y and Zhang C-l, *J. Appl. Polym. Sci.* **131:** 40143 (2014).
6. Chen Y-F, Tan Y-J, Li J, Hao Y-B, Shi Y-D and Wang M, *Polym. Test.* **65:** 387-397 (2018).
7. Shi Y-D, Li J, Tan Y-J, Chen Y-F and Wang M, *Compos. Sci. Technol.* **170:** 70-76 (2019).
8. Li J, Peng W-J, Tan Y-J, Weng Y-X and Wang M, *The Journal of Physical Chemistry C* **123:** 27884-27895 (2019).
9. Raja M, Reddy MJK, Won KH, Kim JI, Cha SH, Bae HN, Song DH, Ryu SH and Shanmugharaj AM. Processing and rheological behaviors of CNT/polymer nanocomposites. In *Rheology and processing of polymer nanocomposites*; Thomas S, Muller R and Abraham J, Ed. Chapter 6; John Wiley & Sons, Inc: Hoboken, New Jersey, 2016; 235-278.
10. Bouhfid R, Essabir H and Qaiss Aek. Graphene-based nanocomposites: mechanical, thermal, electrical, and rheological properties. In *Rheology and processing of polymer nanocomposites*; Thomas S, Muller R and Abraham J, Ed. Chapter 12; John Wiley & Sons, Inc: Hoboken, New Jersey, 2016; 405-429.
11. Martin-Gallego M, Bernal MM, Hernandez M, Verdejo R and Lopez-Manchado MA, *Eur. Polym. J.* **49:** 1347-1353 (2013).
12. Knauert ST, Douglas JF and Starr FW, *J. Polym. Sci., Part B: Polym. Phys.* **45:** 1882-1897 (2007).
13. Nunes MABS, de Matos BR, Silva GG, Ito EN, de Melo TJA and Fechine GJM, *Polym. Compos.* **n/a**2020).
14. Rostami A and Moosavi MI, *J. Appl. Polym. Sci.* **137:** 48520 (2020).
15. Infurna G, Teixeira PF, Dintcheva NT, Hilliou L, La Mantia FP and Covas JA, *Eur. Polym. J.* **133:** 109796 (2020).
16. Feng M, Pan Y, Zhang M, Gao Q, Liu C, Shen C and Liu X, *Compos. Sci. Technol.***:** 108666 (2021).
17. Kim J, Oh J, Lee KY, Jung I and Park M, *Compos. B Eng.* **114:** 445-456 (2017).
18. Cheng HKF, Sahoo NG, Pan Y, Li L, Chan SH, Zhao J and Chen G, *Journal of Polymer Science: Part B: Polymer Physics* **48:** 1203–1212 (2010).
19. Zang C-G, Zhu X-D and Jiao Q-J, *J. Appl. Polym. Sci.* **132:** 41968 (2015).
20. Xiang M, Li C and Ye L, *Journal of Polymer Research* **26:** 104 (2019).
21. Palmer RJ. Polyamides, Plastics. In *Encyclopedia of Polymer Science and Technology*; John Wiley & Sons, Inc., 2002
22. Brydson JA. 18 - Polyamides and Polyimides. In *Plastics Materials (Seventh Edition)*; Butterworth-Heinemann: Oxford, 1999; 478-530.
23. Faghihi M, Shojaei A and Bagheri R, *Compos. B Eng.* **78:** 50-64 (2015).

24. Qiu L, Yang Y, Xu L and Liu X, *Polym. Compos.* **34:** 656-664 (2013).
25. Mayoral B, Harkin-Jones E, Khanam PN, AlMaadeed MA, Ouederni M, Hamilton AR and Sun D, *RSC Advances* **5:** 52395-52409 (2015).
26. Shojaei A, Nourbakhsh P and Faghihi M, *Polym. Adv. Technol.* **25:** 406-417 (2014).
27. Fu X, Yao C and Yang G, *RSC Advances* **5:** 61688-61702 (2015).
28. Caamaño C, Grady B and Resasco DE, *Carbon* **50:** 3694-3707 (2012).
29. Călin MA, Manea LR, Schacher L, Adolphe D, Leon AL, Potop GL and Agop M, *J Nanomater* **2015:** 1-9 (2015).
30. Wang M, Wang W, Liu T and Zhang W-D, *Compos. Sci. Technol.* **68:** 2498-2502 (2008).
31. Doagou-Rad S, Islam A, Jensen JS and Alnasser A, *J. Polym. Eng.* **38:** 971-981 (2018).
32. Sreekanth MS, Panwar AS, Potschke P and Bhattacharyya AR, *Phys. Chem. Chem. Phys.* **17:** 9410-9419 (2015).
33. Zhu X-D, Zang C-G and Jiao Q-J, *J. Appl. Polym. Sci.* **131:** 40923 (2014).
34. Cross MM, *Journal of Colloid Science* **20:** 417-437 (1965).
35. Charman M, Léonardi F, Dominguez S, Bissuel C and Derail C, *J. Polym. Sci., Part B: Polym. Phys.* **49:** 1597-1604 (2011).
36. Nelder JA and Mead R, *The Computer Journal* **7:** 308–313 (1965).
37. Fillon B, Lotz B, Thierry A and Wittmann JC, *J. Polym. Sci., Part B: Polym. Phys.* **31:** 1395-1405 (1993).
38. Fillon B, Wittmann JC, Lotz B and Thierry A, *J. Polym. Sci., Part B: Polym. Phys.* **31:** 1383-1393 (1993).
39. Michell RM, Mugica A, Zubitur M and Müller AJ. Self-Nucleation of Crystalline Phases Within Homopolymers, Polymer Blends, Copolymers, and Nanocomposites. In *Polymer Crystallization I: From Chain Microstructure to Processing*; Auriemma F, Alfonso GC and de Rosa C, Ed. Chapter; Springer International Publishing: Cham, 2017; 215-256.
40. Müller AJ and Arnal ML, *Prog. Polym. Sci.* **30:** 559-603 (2005).
41. Krishnamoorti R and Giannelis EP, *Macromolecules* **30:** 4097-4102 (1997).
42. Sangroniz L, Palacios JK, Fernández M, Eguiazabal JI, Santamaria A and Müller AJ, *Eur. Polym. J.* **83:** 10-21 (2016).
43. Guehenec M, Tishkova V, Dagreou S, Leonardi F, Derail C, Puech P, Pons F, Gauthier B, Cadaux PH and Bacsa W, *J. Appl. Polym. Sci.* **129:** 2527-2535 (2013).
44. Kodgire PV, Bhattacharyya AR, Bose S, Gupta N, Kulkarni AR and Misra A, *Chem. Phys. Lett.* **432:** 480-485 (2006).
45. Abbasi Moud A, Javadi A, Nazockdast H, Fathi A and Altstaedt V, *J. Polym. Sci., Part B: Polym. Phys.* **53:** 368-378 (2015).
46. Krause B, Pötschke P and Häußler L, *Compos. Sci. Technol.* **69:** 1505-1515 (2009).
47. Ning D, Chao-yue Z, Qiao C, Gang W and Rong L, *Mater. Chem. Phys.* **120:** 167-171 (2010).
48. Trujillo M, Arnal ML, Müller AJ, Mujica MA, Urbina de Navarro C, Ruelle B and Dubois P, *Polymer* **53:** 832-841 (2012).